Effect of Familial Parkinson's Disease Point Mutations A30P and A53T on the Structural Properties, Aggregation, and Fibrillation of Human α-Synuclein†

Jie Li,‡,§ Vladimir N. Uversky,*,‡,§,|| and Anthony L. Fink*,§

Department of Chemistry and Biochemistry, University of California, Santa Cruz, California 95064, and Institute for Biological Instrumentation, Russian Academy of Sciences, 142292 Pushchino, Moscow Region, Russia

Received March 27, 2001; Revised Manuscript Received July 30, 2001

ABSTRACT: Parkinson's disease involves the loss of dopaminergic neurons in the *substantia nigra*, leading to movement disorders. The pathological hallmark of Parkinson's disease is the presence of Lewy bodies and Lewy neurites, which are intracellular inclusions consisting primarily of α-synuclein. Although essentially all cases of sporadic and early-onset Parkinson's disease are of unknown etiology, two point mutations (A53T and A30P) in the α-synuclein gene have been identified in familial early-onset Parkinson's disease. Previous reports have shown that mutant α-synuclein may form fibrils more rapidly than wild-type protein. To determine the underlying molecular basis for the enhanced fibrillation of the mutants, the structural properties, responses to changes in the environment, and propensity to aggregate of wild-type, A30P, and A53T α-synucleins were systematically investigated. A variety of biophysical methods, including far-UV circular dichroism, FTIR, small-angle X-ray scattering, and light scattering, were employed. Neither the natively unfolded nor the partially folded intermediate conformations are affected by the familial Parkinson's disease point mutations. However, both mutants underwent self-association more readily than the wild type (i.e., at much lower protein concentration and more rapidly). We attribute this effect to the increased propensity of their partially folded intermediates to aggregate, rather than to any changes in the monomeric natively unfolded species. This increased propensity of these mutants to aggregate, relative to wild-type α-synuclein, would account for the correlation of these mutations with Parkinson's disease.

Parkinson's disease (PD)[1] is the second most common neurodegenerative disorder, after Alzheimer's disease, affecting approximately 0.2% of the population. However, since it is predominantly an "aging" disease, the prevalence is much higher in the population over 60 years old. Clinically, it is a movement disorder characterized by tremor, rigidity, and bradykinesia. These symptoms are attributed to the progressive loss of dopaminergic neurons from the *substantia nigra* region of the brain. Some surviving nigral dopaminergic neurons contain cytosolic filamentous inclusions known as Lewy bodies and Lewy neurites (*1*, *2*). In addition to the *substantia nigra*, LBs and LNs also are found in other brain regions, such as the dorsal motor *nucleus of the vagus*, the *nucleus basalis of Meynert*, and the *locus coeruleus* (*2*). Abundant LBs and LNs in the cerebral cortex are also neurophathological hallmarks of dementia with Lewy bodies (DLB), a common late-life dementia that is clinically similar to AD (*3*). Furthermore, LBs and α-synuclein were detected in the Lewy body variant of Alzheimer's disease (LBVAD) (*4*). Structurally, typical LBs appear as intracytoplasmic inclusions, 5−25 μm in diameter with a dense eosinophilic core and clearer surrounding halo. Ultrastructurally, they are composed of a dense core of filamentous and granular material that is surrounded by radially oriented filaments (*5*).

Several observations have implicated the presynaptic protein α-synuclein in the pathogenesis of PD. First, α-synuclein was shown to be a major fibrillar component of LBs and LNs (*6*, *7*). Second, two different missense mutations in the α-synuclein gene, corresponding to A53T and A30P substitutions in α-synuclein, have been identified in two kindreds with autosomal-dominantly inherited, early-onset PD (*8*, *9*). Finally, the production of wild-type (WT) α-synuclein in transgenic mice (*10*) or of WT, A30P, and A53T in transgenic flies (*11*) leads to the motor deficits and neuronal inclusions reminiscent of PD.

α-Synuclein is a small (14 kDa), highly conserved protein that is abundant in various regions of the brain (*12*−*15*). The level of α-synuclein increases during the early stages of postnatal murine brain development (*16*) and during the critical period for song learning in zebra finch (*15*), suggesting a role of the protein in the synaptic development, function, and plasticity. The amino acid sequence of α-sy-

† This research was supported by a grant from the National Institutes of Health. V.N.U. was supported by fellowships from the Parkinson's Institute and the National Parkinson's Foundation.

* To whom correspondence should be addressed. Fax: +1-831-459-2935. E-mail: enzyme@cats.ucsc.edu.

‡ These authors made equal contributions.

§ University of California, Santa Cruz.

|| Russian Academy of Sciences.

[1] Abbreviations: PD, Parkinson's disease; LB, Lewy body; LN, Lewy neurite; DLB, dementia with LB; AD, Alzheimer's disease; LBVAD, LB variant of AD; CD, circular dichroism; UV, ultraviolet; FTIR, Fourier transform infrared; SAXS, small-angle X-ray scattering; PAGE, polyacrylamide gel electrophoresis; EM, electron microscopy; AFM, atomic force microscopy; WT, human recombinant wild-type α-synuclein; A30P, human recombinant A30P α-synuclein; A53T, human recombinant A53T α-synuclein; TFT, thioflavin T; CBD, chitin-binding domain.

10.1021/bi010616g CCC: $20.00
Published on Web 08/28/2001

nuclein is characterized by six imperfect repeats (consensus KTKEGV) within the N-terminal part of the polypeptide (residues 1−95), as well as by an acidic carboxyl-terminal region (residues 96−140) (*13*, *17*). Structurally, purified α-synuclein belongs to the rapidly growing family of natively unfolded proteins, which have little or no ordered structure under physiological conditions (*18*, *19*). This lack of folded structure has been shown to correlate with specific combinations of low overall hydrophobicity and large net charge (*20*).

The A30P and A53T α-synucleins have also been shown to be natively unfolded under physiological conditions (*21*). The aggregation behavior of the recombinant α-synucleins has been studied under physiological conditions in vitro. It has been established that all three proteins, as well as the 1−87 and 1−120 truncated forms, are able to assemble readily into filaments, with morphologies and staining characteristics similar to those extracted from the disease-affected brain (*19*, *21*−*29*). Fibrillation occurs via a nucleation-dependent mechanism (*26*, *28*) with the critical primary stage being the structural transformation of the protein from the unfolded conformation to a partially folded intermediate (*19*).

Despite these studies, little is currently known about the structural basis for the difference in the fibrillation capabilities between wild-type α-synuclein and its A30P and A53T mutants. The major question is how a single point mutation in the disordered ("natively unfolded") conformation can affect the aggregation and fibrillation properties of the protein.

Here, we describe the effect of the familial point mutations A30P and A53T on the structural properties of α-synuclein under different experimental conditions, on the apparent "stability" of the protein, and on the aggregation and fibrillation properties of α-synuclein in vitro.

EXPERIMENTAL PROCEDURES

Materials. Thioflavin T was obtained from Sigma, St. Louis, MO. All other chemicals were of analytical grade from Fisher Chemicals.

Expression and Purification of WT, A30P, and A53T α-Synucleins. WT α-synuclein and its A30P and A53T mutants were produced and purified by fusing their genes to a CBD/intein system (IMPACT T7 one-step protein purification system, New England Biolabs) and expressing the fusion proteins in *Escherichia coli*. This system allowed simple purification of α-synucleins by binding of the CBD-fusion proteins to a chitin column, followed by addition of a thiol agent (DTT or cysteine) to induce the cleavage reaction of the intein and release the α-synucleins. The purity of the resultant proteins was assessed by PAGE, gel filtration, and electrospray mass spectrometry.

Fibril Formation. Solutions of 0.5 mL of α-synucleins at pH 7.5 in 20 mM Tris and 150 mM NaCl buffer were stirred at 37 °C in glass vials with micro stir bars. The advantage of stirring the samples is that the kinetics of fibril formation are significantly increased. We believe this is due to interactions of the protein at the air/water interface, leading to population of the partially folded intermediate. Protein concentrations were 1 mg/mL. Fibril formation was monitored with thioflavin T fluorescence (*30*, *31*): aliquots of 10 μL were removed from the incubated sample at predetermined time points and added to 1.0 mL of 20 μM TFT in 20 mM Tris buffer, pH 8.0. Experiments were run in at least triplicate and averaged. The presence of fibrils was confirmed by EM (negative staining with uranyl acetate) and AFM.

Data Evaluation of Fibrillation Kinetics. The kinetics of α-synuclein fibril formation are defined by an initial lag phase, where no change in TFT fluorescence intensity was observed, a subsequent growth phase, in which TFT fluorescence increased, and a final equilibrium phase, where TFT fluorescence reached a plateau, indicating the end of fibril formation. For purposes of comparing kinetic parameters the TFT kinetics were analyzed with a sigmoidal curve described by the equation:

$$Y = (y_i + m_i t) + \frac{(y_f + m_f t)}{1 + e^{-[(t - t_m)/\tau]}}$$

where Y is the fluorescence intensity at time t, and t_m is the time to 50% of maximal fluorescence. The apparent first-order rate constant, k_{app}, for the growth of fibrils is $1/\tau$, and the lag time is given by $t_m - 2\tau$.

Light Scattering Measurements. Rayleigh light scattering at 330 nm was used to monitor the total aggregation as a function of time. Although these experiments are not quantitative, if the light scattering precedes fibril formation, it indicates the buildup of other types of aggregates, e.g., soluble oligomers.

Circular Dichroism Measurements. CD spectra were obtained on an AVIV 60DS spectrophotometer (Lakewood, NJ) using α-synuclein concentrations of ∼0.5 mg/mL. Spectra were recorded using a 0.01 cm cell from 250 to 190 nm with a step size of 0.5 nm, a bandwidth of 1.5 nm, and an averaging time of 10 s. For all spectra, an average of five scans was obtained. CD spectra of the appropriate buffers were recorded and subtracted from the protein spectra.

Fluorescence Measurements. Fluorescence measurements were performed in semimicro quartz cuvettes (Hellma) with a 1 cm excitation light path using a FluoroMax-2 spectrofluorometer from Instruments S.A., Inc., Jobin Yvon-Spex. The light source was a 150 W xenon lamp. TFT fluorescence was recorded immediately after addition of protein aliquots to the TFT mixture from 470 to 560 nm with excitation at 450 nm, an increment of 1 nm, an integration time of 1 s, and slits of 5 nm for both excitation and emission. For each sample the signal was obtained as the TFT intensity at 482 nm from which was subtracted a blank measurement recorded prior to addition of α-synuclein to the TFT solution. All data were processed using DataMax/GRAMS software.

FTIR Spectra. Data were collected on a Nicolet 800SX FTIR spectrometer equipped with an MCT detector. The IRE (72 × 10 × 6 mm, 45° germanium trapezoid) was held in a modified SPECAC out-of-compartment ATR apparatus. The hydrated thin films were prepared and analyzed as described previously (*32*, *33*). Typically 1024 interferograms were coadded at 4 cm^{-1} resolution. Data analysis was performed with GRAMS32 (Galactic Industries). Secondary structure content was determined from curve fitting to spectra deconvoluted using second derivatives and Fourier self-deconvolution to identify component band positions.

SAXS Experiments. Small-angle X-ray scattering (SAXS) measurements were made using Beam Line 4-2 at the Stanford Synchrotron Radiation Laboratory (*34*). X-ray

energy was selected at 8980 eV (Cu edge) by a pair of Mo/B_4C multilayer monochromator crystals (*35*). To avoid radiation damage of the sample in SAXS measurements, the protein solution was continuously passed through a 1.3 mm path length observation flow cell with 25 μm mica windows. Background measurements were performed before and after each protein measurement and then averaged before being used for background subtraction. All SAXS measurements were performed at 23 ± 1 °C.

The radius of gyration (R_g) was calculated according to the Guinier approximation (*36*):

$$\ln I(Q) = \ln I(0) - R_g^2 Q^2/3$$

where Q is the scattering vector given by $Q = (4\pi \sin \theta)/\lambda$ (2θ is the scattering angle, and λ is the wavelength of X-ray). $I(0)$, the forward scattering amplitude, is proportional to $n\rho_c^2V^2$, where n is the number of scatters (protein molecules) in solution, ρ_c is the electron density difference between the scatter and the solvent, and V is the volume of the scatter. This means that the value of forward-scattered intensity, $I(0)$, is proportional to the square of the molecular weight of the molecule (*36*). Thus, $I(0)$ for a pure N-mer sample will therefore be N-fold that for a sample with the same number of monomers since each N-mer will scatter N^2 times as strongly as monomer, but in this case the number of scattered particles (N-mers) will be N times less than that in the pure monomer sample.

Transmission Electron Microscopy (TEM). Samples of α-synuclein fibrils were placed onto glow discharged carbon grids, rinsed with 0.1 M KCl, and negatively stained with 1% uranyl acetate. The specimens were viewed, and images recorded, with a Philips 208 electron microscope operated at 80 kV.

RESULTS

We have previously shown that the process of α-synuclein fibrillation may be minimally presented by the scheme (*19*):

$$U_N \leftrightarrows I \leftrightarrows Nucl \rightarrow F$$

where U_N, I, Nucl, and F correspond to natively unfolded conformation, partially folded intermediate, fibril nucleus, and fibril, respectively. From this model the structural transformation leading to the intermediate and the formation of the nucleus represent two key kinetic steps. Thus, factors that shift the equilibrium in favor of the intermediate and/or nucleus may facilitate fibril formation. We anticipate that the familial Parkinson's disease point mutations, A30P and A53T, which have been shown to increase the rate of α-synuclein aggregation (*21*, *23*−*25*, *27*, *28*), will change the structural properties of the protein at the stages U_N and/or I. These structural changes could result in a shift of the equilibrium toward the intermediate and/or nucleus, thus accelerating the fibril formation. To check this assumption, the structural properties of WT, A30P, and A53T α-synucleins in their U_N and I states have been compared.

Effect of pH on the Far-UV CD Spectra of WT, A30P, and A53T a-Synucleins. Figure 1 represents the far-UV CD spectra of human recombinant α-synucleins (WT, A30P, and A53T) measured at pH 7.5 (open symbols) and pH 3.0 (closed symbols) at 20 °C. At neutral pH, all three proteins possess almost indistinguishable far-UV CD spectra, which are typical of an essentially unfolded polypeptide chain, including the characteristic minima in the vicinity of 196 nm and the absence of bands in the 210−230 nm region. As the pH is decreased, changes are observed in the spectral shape for all three proteins. Figure 1 shows that the decrease in the minimum at 196 nm is accompanied by an increase in negative intensity around 222 nm, reflecting pH-induced formation of secondary structure. Interestingly, all three proteins possess almost identical far-UV CD spectra at acidic pH.

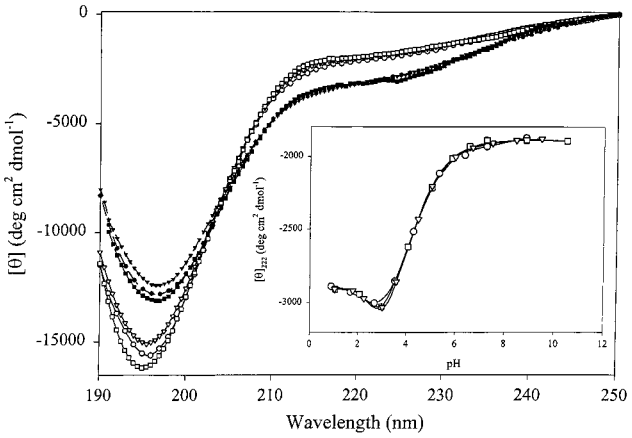

FIGURE 1: Comparison of the effect of pH on far-UV CD spectra of α-synuclein (circles) and its A30P and A53T mutants (inverted triangles and squares, respectively). Far-UV CD spectra were measured at pH 8.5 (open symbols) and pH 2.9 (closed symbols). The inset represents the pH dependence of $[\theta]_{222}$. For far-UV CD measurements the cell path length was 0.1 mm. Measurements were carried out at 23 °C. The protein concentration was 0.2 mg/mL.

The pH dependency of $[\theta]_{222}$ for the three proteins is shown in the inset to Figure 1. The data show that WT, A30P, and A53T behave similarly and that the pH-induced changes in the far-UV CD of all three proteins are completely superimposable. There is little change in the far-UV CD spectrum between pH ∼9.0 and pH ∼5.5. However, a decrease in pH from 5.5 to 3.0 results in an ∼2-fold increase in negative intensity in the vicinity of 220 nm, and a further decrease in pH is accompanied by a reversal in the spectral intensity. Additionally, the pH-induced changes in the far-UV CD spectra of the α-synucleins were completely reversible. Previously, we have shown that the pH-induced increase in structure of WT α-synuclein represents an intramolecular process involving the formation of a partially folded intermediate and not self-association (*19*). Thus, this also appears to be the situation for the A30P and A53T mutants.

Small Angle X-ray Scattering Analysis of WT, A30P, and A53T at Different pHs. Small-angle X-ray scattering (SAXS) is excellent method for the investigation of conformation, shape, and association of biopolymers in solution. Analysis of the scattering curves using the Guinier approximation gives information about the radius of gyration, R_g. Presentation of the scattering data in the form of Kratky plots provides information about the globularity (packing density) and conformation of a protein (*36*). For a native globular protein this plot has a characteristic maximum, whereas unfolded and partially folded polypeptides have significantly different-shaped Kratky plots.

Guinier analysis of the scattering data shows that at neutral pH WT α-synuclein and its A30P and A53T mutants have

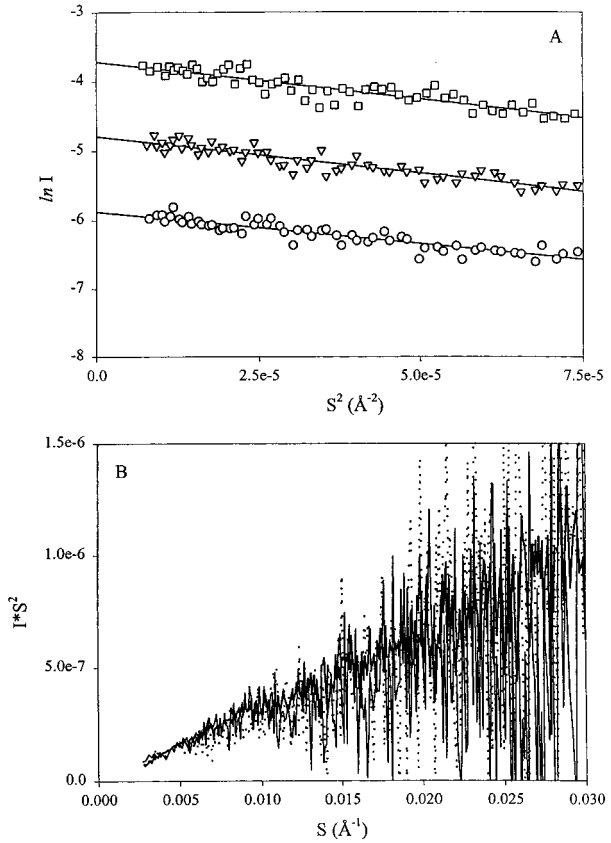

FIGURE 2: Guinier (A) and Kratky plot (B) representation of the results of small-angle X-ray scattering analysis of α-synucleins at pH 7.5. Data for the WT protein are shown by circles (A) and a solid line (B). Results for the A30P mutant are shown by inverted triangles (A) and a dotted line (B). Data for the A53T mutant are shown by squares (A) and a dashed line (B). Measurements were carried out at pH 7.5 and 23 °C. The protein concentration was 0.5 mg/mL.

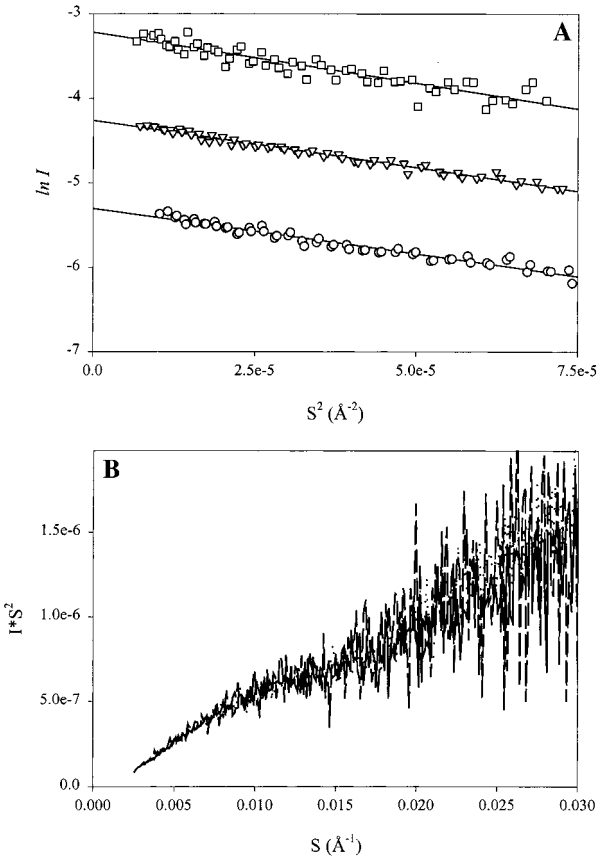

FIGURE 3: Guinier (A) and Kratky plot (B) representation of the results of small-angle X-ray scattering analysis of α-synucleins at pH 3.0. Data for the WT protein are shown by circles (A) and a solid line (B). Results for the A30P mutant are shown by inverted triangles (A) and a dotted line (B). Data for the A53T mutant are shown by squares (A) and a dashed line (B). Measurements were carried out at pH 3.0 and 23 °C. The protein concentration was 0.5 mg/mL.

identical values of R_g, namely, 40 ± 1 Å (Figure 2A). For all three proteins this value decreases to 30 ± 1 Å at pH 3.0, reflecting substantial compaction of the protein, corresponding to a volume decrease of 2.4-fold (see Figure 3A). The linear Guinier plots indicate that the solutions of these three proteins are homogeneous under the conditions studied and that there is no aggregation present. The observed R_g values for the α-synucleins at neutral pH (40 Å) are smaller than those estimated for a random coil conformation for a protein of this size (52 Å), indicating that the natively unfolded conformations of all three proteins are more compact than that of a random coil. On the other hand, the R_g for the partially folded intermediates at low pH (30 Å) is much larger than that of a folded globular protein of the size of α-synuclein (15 Å) (*19*).

Analysis of the X-ray scattering in the form of a Kratky plot shows that the α-synucleins do not have well-developed globular structure at either pH 7.5 or pH 3.0 (Figures 2B and 3B). However, whereas the profiles of the Kratky plots at neutral pH are typical for a random coil conformation, those at pH 3 show changes consistent with the genesis of a tightly packed core.

The SAXS forward-scattering intensity values, $I(0)$, give information on the degree of protein association. Our data indicate that on decreasing the pH there is no significant change in this parameter for WT, A30P, or A53T α-synucleins. This directly confirms that the pH-induced folding of these proteins is an intramolecular process and does not result from self-association (at the concentration of 0.5 mg/mL used).

Effect of Temperature on the Far-UV CD Spectra of WT, A30P, and A53T a-Synucleins. Figure 4 represents the far-UV CD spectra of WT, A30P, and A53T α-synucleins measured at 3 and 95 °C at pH 7.5. Spectra obtained for WT at pH 3.0 and different temperatures are shown for comparison. At low temperatures all three proteins possess far-UV spectra typical of an unfolded polypeptide chain. As the temperature increases, the spectra undergo changes consistent with temperature-induced formation of secondary structure. The temperature dependence of $[\theta]_{222}$ (inset to Figure 4) shows that at pH 7.5 the major spectral changes occur over the range of 3−50 °C for all three α-synucleins. Further heating leads to a less pronounced effect. A similar increase in secondary structure is observed at pH 3.0 (see inset to Figure 4). Interestingly, the difference between $[\theta]_{222}$ measured for the proteins at pH 7.5 and 3.0 increases with temperature. The structural changes induced in WT, A30P, and A53T by heating were completely reversible (data not shown). These data are consistent with the conclusion that both heating and decrease in pH contribute to the reversible transformation of α-synucleins to a partially folded intermediate.

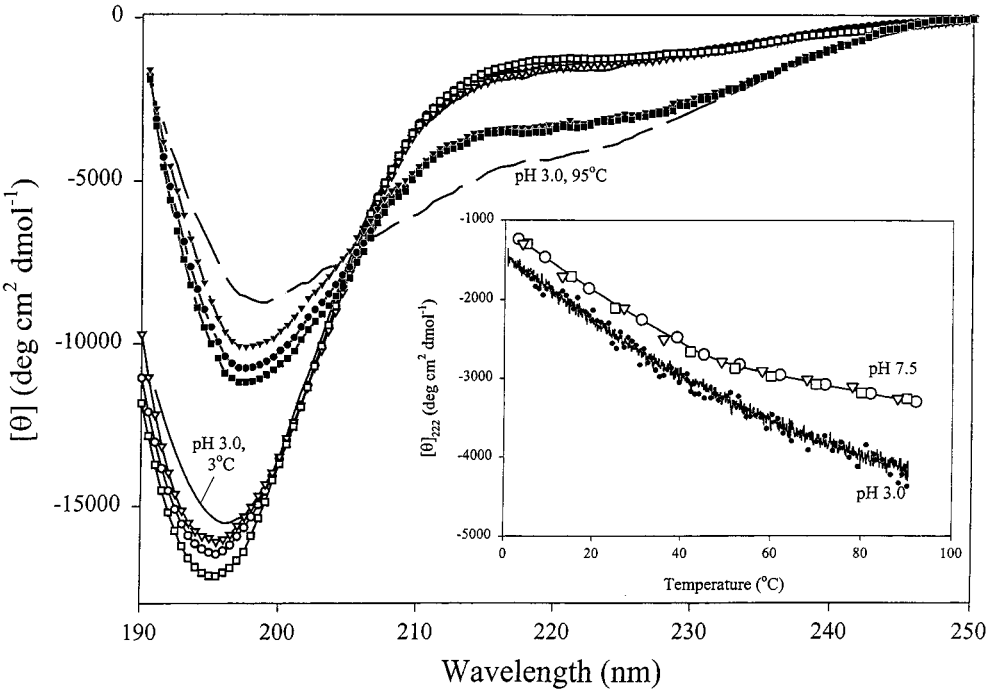

FIGURE 4: Comparison of the effect of temperature on the far-UV CD spectra of α-synuclein (circles) and its A30P and A53T mutants (inverted triangles and squares, respectively). Far-UV CD spectra were measured at 3 °C (open symbols) and 95 °C (closed symbols). The inset represents the temperature dependence of $[\theta]_{222}$ measured at pH 7.5 (all proteins) and pH 3.0 (WT, solid line, and A30P, circles). Measurements were carried out in a 0.1 mm cell. The protein concentration was 0.2 mg/mL.

Effect of Methanol on the Far-UV CD Spectra of WT, A30P, and A53T. Since α-synuclein may interact with lipid membranes (*57*), we investigated the effect of decreasing the polarity and dielectric constant of the solvent on the structure of α-synuclein and its mutants. Figure 5 shows the far-UV CD spectra of WT, A30P, and A53T α-synucleins measured at pH 7.5 and 23 °C in the absence or presence of 80% methanol. There are two points to note; first, all three proteins had similar spectra, and, second, the presence of the alcohol induced substantial secondary structure. In fact, the spectra measured in the presence of 80% methanol are typical of folded proteins with well-developed secondary structure (in particular, β-structure). Figure 5B compares methanol-induced changes in the $[\theta]_{222}$ value for α-synucleins. All three proteins showed an identical response to the increasing methanol content, showing superimposable $[\theta]_{222}$ vs methanol concentration dependencies. The methanol-induced structural changes were not reversible on diluting out the methanol, suggesting that association had occurred. Interestingly, similar studies performed at higher protein concentrations (>1.0 mg/mL) were accompanied by detectable protein precipitation. Thus in the presence of methanol, WT, A30P, and A53T α-synucleins undergo a conformational change and self-associate to form oligomers, which aggregate and form insoluble precipitates at higher concentrations.

The capacity of concentrated organic solvents to induce structural changes (often, denaturation accompanied by an increase in content of α-helical conformation) in native globular proteins is well established (*37*−*51*). Much less is currently known about the behavior of natively unfolded proteins in water/organic mixtures (*52*−*56*); however, one would expect similar effects. For α-synuclein it has been shown that solutions containing fluorinated alcohols, or detergent micelles (*18*, *21*), or small unilamellar vesicles (*57*) induce α-helical structure. Contrary to these observations, our data show that, in the neutral methanol solutions, WT α-synuclein and its A30P and A53T mutants form soluble and insoluble aggregates, enriched with β-structure. It is not possible at this stage to determine whether the β-structure arises from the intermolecular interactions formed in the association of the intermediate or is present in the intermediate itself.

Secondary Structure Analysis by FTIR. A major advantage of FTIR in comparison with CD is that FTIR is much more sensitive to β-structure. Experiments with relatively low protein concentrations were performed using attenuated total reflectance FTIR and hydrated thin films of the sample (*32*, *33*). Figure 6 shows the FTIR (amide I region) spectra measured for WT (Figure 6A), A30P (Figure 6B), and A53T α-synuclein (Figure 6C) at pH 7.5. The FTIR spectrum of WT protein is typical of a substantially unfolded polypeptide chain, whereas spectra of A30P and A53T possess significant changes, indicative of increased ordered structure. The most evident change is the appearance of a new band in the vicinity of 1626 cm^{-1}, which corresponds to β-sheet. This means that mutant α-synucleins contain significant amounts of β-structure under these conditions. As discussed below, this is due to association at the protein concentrations used in the FTIR experiments.

Deconvolution (FSD and second derivative) of the FTIR spectra, followed by curve fitting, permitted quantitation of the differences in the secondary structure in WT, A30P, and A53T. These results are summarized in Table 1. The β-structure content of the α-synucleins increases in the following order: WT < A30P < A53T. Table 1 shows that the β-sheet content of the mutants is 1.54 (A30P) and 1.85 times (A53) greater that that of the WT protein.

This is a rather unexpected observation, as all three proteins possess almost identical far-UV CD spectra. The

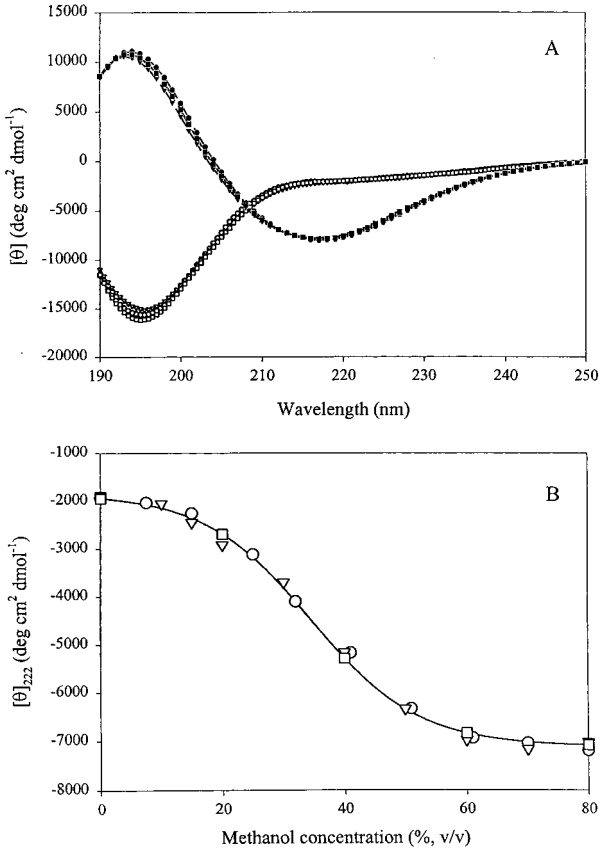

FIGURE 5: Comparison of the effect of methanol on the far-UV CD spectra of α-synuclein (circles) and its A30P and A53T mutants (inverted triangles and squares, respectively). (A) Representative far-UV CD spectra measured at 0 (open symbols) and 80% methanol (closed symbols). (B) Methanol-induced changes in $[\theta]_{222}$ values, measured at pH 7.5 (all proteins) and pH 3.0 (WT, solid line, and A30P, circles). Measurements were performed at pH 7.5 and 23 °C in a 0.1 mm cell. The protein concentration was 0.2 mg/mL.

source of this apparent discrepancy between CD and FTIR data is due to the difference in the protein concentration used in the two types of experiments. The far-UV CD measurements were performed in dilute protein solutions (0.2 mg/mL), whereas the hydrated thin film samples analyzed by FTIR had much higher concentrations (≥1 mg/mL). Thus the combined CD and FTIR data indicate that the mutants have a greater propensity to aggregate at higher concentrations than the wild-type protein; this was further confirmed as follows.

Effect of Protein Concentration on the Far-UV CD Spectra. To investigate if there were differences in the propensity of the mutants to aggregate, we investigated the concentration dependence of the circular dichroism spectra. Figure 7 shows far-UV CD spectra for the three α-synucleins measured at different protein concentrations, and the inset shows the $[\theta]_{222}$ vs protein concentration dependencies. These data support the hypothesis that the major difference between WT, A30P, and A53T α-synucleins is their propensity to aggregate, since the spectral changes are attributed to intermolecular association of the partially folded intermediate. In fact, the far-UV CD spectrum of WT is invariant within a wide range of protein concentrations (0.1−8.0 mg/mL), whereas spectra of both mutants show strong concentration dependence, with A53T being the most sensitive.

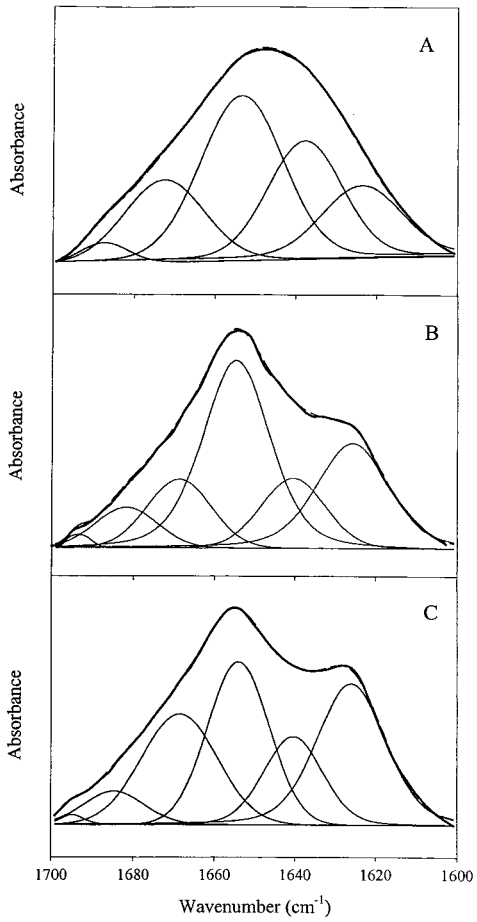

FIGURE 6: Secondary structure analysis of WT α-synuclein (A) and its A30P (B) and A53T (C) mutants by FTIR. FTIR spectra of the amide I region were measured at pH 7.5 (solid line). Curve fit spectra are presented by dashed lines. The major β-structure bands are in the 1620−1640 cm^{-1} region.

Table 1: Secondary Structure Analysis of Human α-Synuclein and Its A30P and A53T Mutants Determined by FTIR[a]

	WT		A30P		A53T	
structural assignment	wave-number (cm^{-1})	%	wave-number (cm^{-1})	%	wave-number (cm^{-1})	%
turn	1688	2.9	1682	7.3	1685	5.5
turn	1673	18.5	1669	12.9	1669	23.2
loops/disordered	1655	38.3	1655	42.2	1654	27.7
extended[b]	1640	24.7	1641	13.5	1640	14.8
β-sheet	1626	15.6	1626	24.1	1626	28.8

[a] The estimated error in the frequencies is ± 1.5 cm^{-1}. [b] The assignment of this band is uncertain; it may also reflect disordered secondary structure or a combination of extended and disordered.

Differences between WT, A30P, and A53T in Aggregation and Fibrillation. TFT is a fluorescent dye, which interacts rather specifically with fibrils and not with most native proteins or amorphous aggregates. Binding of TFT to protein fibrils is accompanied by a characteristic increase in the fluorescence intensity in the vicinity of 480 nm (*30*, *31*). In work to be reported elsewhere we have shown that the rate of α-synuclein fibril formation increases as the protein concentration is increased: both the lag time decreases and the growth rate increases, leading to a decrease in the midpoint of the fibrillation transition. Figure 8A compares fibrillation patterns of WT, A30P, and A53T α-synucleins

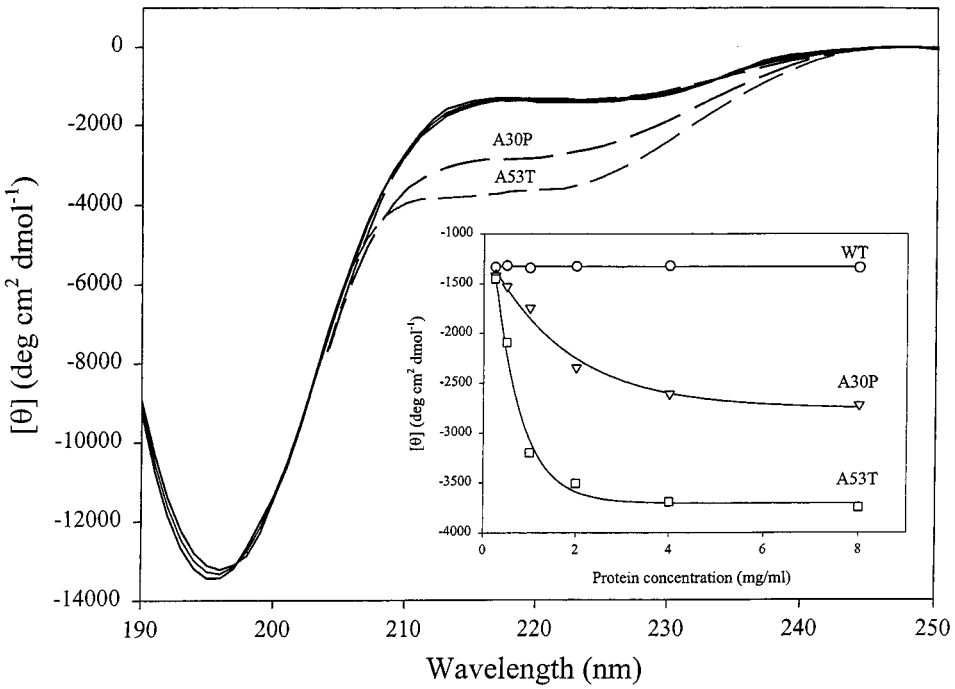

FIGURE 7: Effect of protein concentrations on the far-UV CD spectra of α-synuclein (circles) and its A30P and A53T mutants (inverted triangles and squares, respectively). Representative far-UV CD spectra were measured at 0.1 (solid lines) and 4.0 mg/mL (dashed lines). The inset represents the dependence of $[\theta]_{222}$ on protein concentration. Measurements were performed at pH 7.5 and 23 °C in cells with path lengths of 1.0 and 0.1 mm for low and high protein concentrations, respectively.

monitored by TFT fluorescence. In agreement with earlier studies (*21*, *24*), A53T shows the fastest rate of fibril formation, whereas A30P forms fibrils more slowly than the WT protein.

It is known that static light scattering from protein solutions reflects the formation of large particles; i.e., this is an association-dependent parameter. In contrast to TFT, the increase in static light scattering will reflect the formation of all large particles, both fibrillar and amorphous (including large soluble oligomers). To compare the total aggregation rates of WT, A30P, and A53T α-synucleins, time courses of static light scattering were studied. Figure 8B shows that both mutants are more prone to aggregate than WT protein. The total aggregation rates decrease in the following order: A53T > A30P > WT. Interestingly, the three proteins differed not only in their rates of aggregation but also in their final light scattering signal, which showed the A53T > WT > A30P pattern. (Note, this is the pattern for total aggregation, not fibrillation. The A30P mutant forms non-fibrillar aggregates much faster than it forms fibrils.) This may reflect essential differences between the three proteins in terms of the number of aggregates and/or the size of the aggregates. In addition, the light scattering preceded the formation of fibrils, as monitored by TFT, consistent with formation of soluble oligomers, which could be on or off the fibrillation pathway.

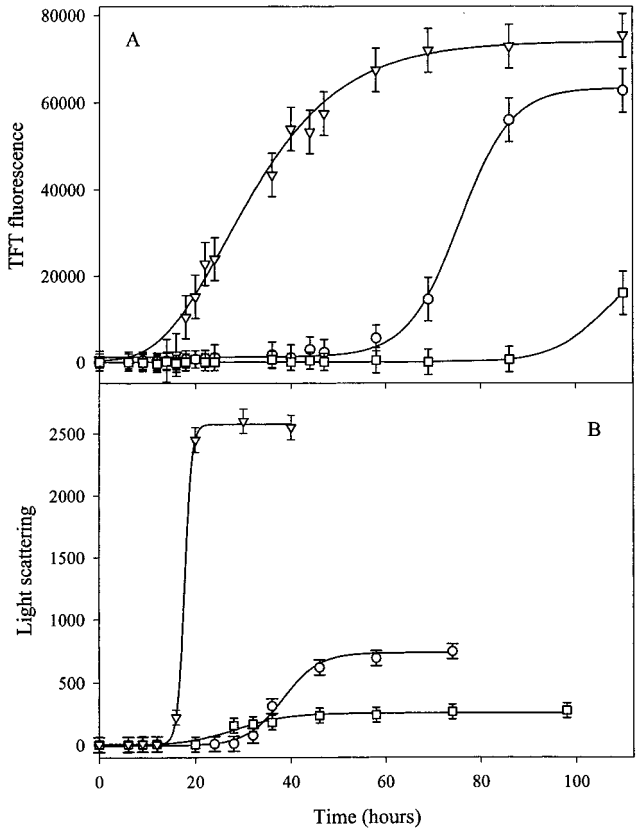

FIGURE 8: Kinetics of fibrillation (A) and aggregation (B) of α-synucleins monitored by the enhancement of thioflavin T fluorescence intensity and light scattering, respectively. Measurements were performed at 37 °C for WT (circles), A53T (inverted triangles), and A30P (squares) proteins. TFT fluorescence was excited at 450 nm, and the emission wavelength was 482 nm. Light scattering measurements were performed at 330 nm.

DISCUSSION

Our data indicate that WT, A30P, and A53T α-synucleins possess similar structural properties (cf. ref *21*). Furthermore, the conformational transitions induced in these three proteins by decrease in pH or increases in temperature or methanol concentration are indistinguishable. Likewise, the WT (*19*), A30P, and A53T mutants may be transformed into the

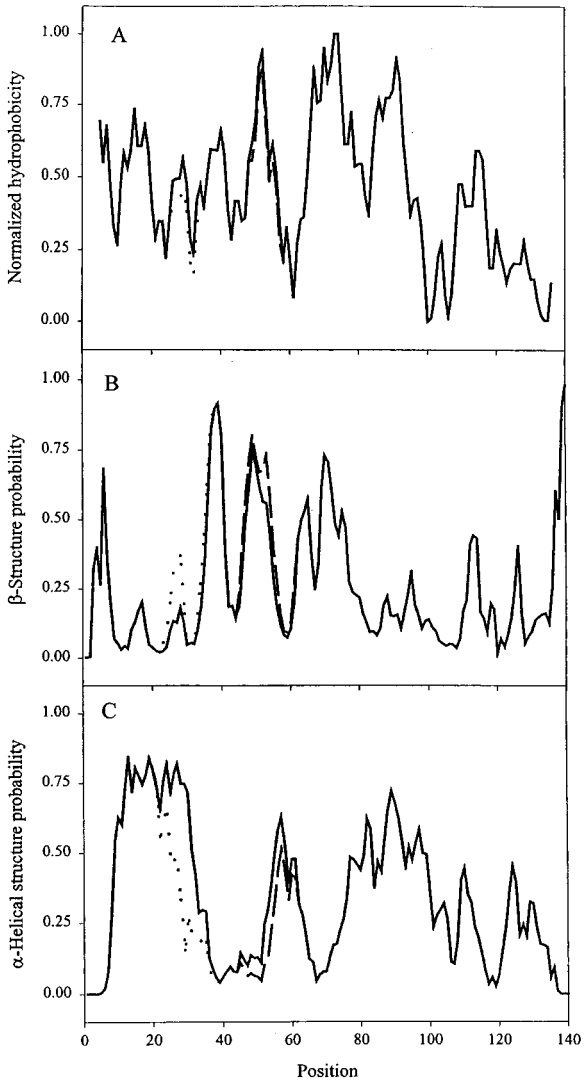

FIGURE 9: Distribution of hydrophobicity (A) and probability to form the β-sheet (B) or α-helical structure (C) throughout the amino acid sequences of WT α-synuclein (solid line) and its A30P (dotted line) and A53T (dashed line) mutants. Hydrophobicity of proteins was calculated according to the Kyte and Doolittle approach (*67*), whereas the probability for β-sheet or α-helical structure was calculated using the hierarchical neural network method (*68*).

partially folded intermediate state by decreasing the pH or increasing the temperature. Importantly, the structure of this intermediate state is independent of the mutations. Thus the monomeric forms of WT, A30P, and A53T α-synucleins exhibit identical structural properties and conformational behavior. On the other hand, the data show that the propensity to aggregate of α-synuclein is strongly enhanced by the familial Parkinson's disease point mutations (cf. refs *21*, *23*, and *24*). Recently, we proposed a model for the fibrillation of α-synuclein in which the first step is the conformational transformation of the natively unfolded protein into the aggregation-competent partially folded intermediate (*19*). The absence of any detectable structural difference between partially folded conformations of α-synucleins raises the question of how point mutations may affect the aggregation propensity of the protein.

To further improve our understanding, we analyzed the amino acid sequence of WT, A30P, and A53T. Figure 9 compares sequences of these proteins in scales of hydrophobicity (Figure 9A) and propensity to form β-sheet (Figure 9B) or α-helix (Figure 9C). Figure 9A shows that the hydrophobicity of both mutants is slightly reduced in the vicinity of both substitutions. This is an interesting observation, in that hydrophobic interactions are assumed to be important in aggregation, and so we have the apparent paradox that a decrease in hydrophobicity is associated with increased aggregation propensity.

Scheme 1

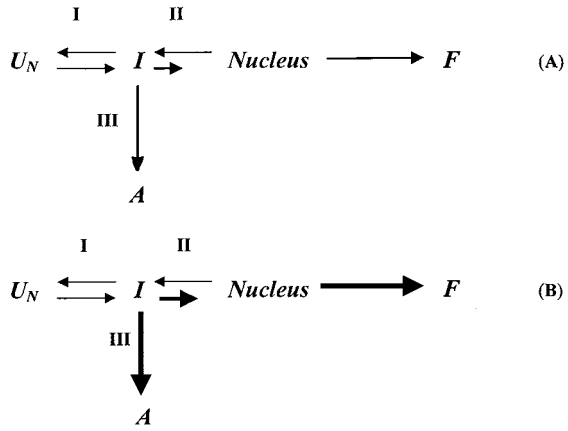

Figure 9C shows that the propensity to form α-helical structure is somewhat diminished in the N-terminal region of both mutants. Since this region is believed to be involved in binding to lipids, this may also play a role in the physiological consequences of the mutations. Both A30P and A53T are predicted to be more likely to form β-structure than WT α-synuclein (Figure 9B). The aggregated species of many proteins are enriched in β-structure. Moreover, it has been established that transformation of α-helical (or disordered) structure to β-sheets (including intermolecular ones) is a hallmark of aggregation and fibrillation processes (*32*, *60*−*66*). Taking these observations into account, we hypothesize that the increased internal susceptibility of A30P and A53T to form β-sheets may not be strong enough to alter the structure of the monomeric proteins but may affect the aggregation behavior of the α-synuclein mutants through specific stabilization of an intermolecular β-structure. This model for the effect of the familial Parkinson's disease mutations is illustrated by comparison of the aggregation models for the WT (A) and the mutants (B) in Scheme 1. In this model F and A represent fibrils and amorphous aggregates (or soluble oligomers), respectively, U_N is the natively unfolded state, and I represents the partially folded intermediate. The Roman numerals indicate the major stages of the aggregation process. A number of observations indicate that α-synuclein can form both fibrils and amorphous aggregates under some conditions. For example, Figure 8 suggests the formation of large oligomeric species significantly earlier than fibrils, and the fact that monomers of A30P disappear more rapidly than fibrils appear (*28*) is consistent with nonfibrillar aggregates. Confirmation of the presence of amorphous aggregates, along with fibril deposits from α-synuclein, was observed by electron microscopy (Figure 10).

In the above model we propose that the structural properties of U_N and I, as well as the rate of their interconversion (stage I), are unaffected by the A30P and A53T mutations. However, the rates of stages II and III are facilitated by the familial Parkinson's disease point mutations

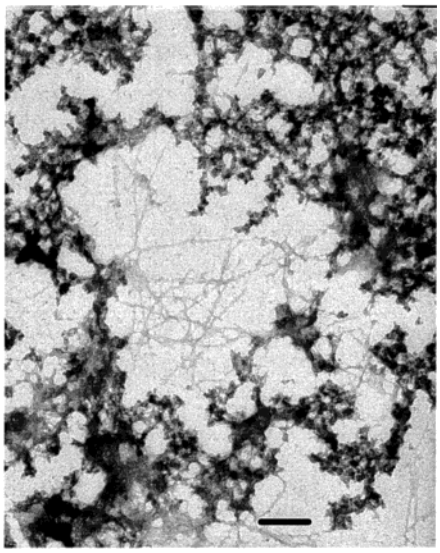

FIGURE 10: Negatively stained transmission electron micrograph of aggregated α-synuclein. Both fibrils and amorphous aggregates can be seen. Depending on the experimental conditions the ratio of fibrils to amorphous aggregate varies. The image is at 32000× magnification. The scale bar is 200 nm. The sample was wild-type α-synuclein incubated at 37 °C.

(thicker arrows). This would result from the mutation-enhanced probability of forming intermolecular β-structure. As a result, the mutants show a faster rate of fibrillation (A53T) or amorphous aggregation or soluble oligomers (A30P).

Our results showing that the A53T and A30P mutations in α-synuclein lead to increased propensity to aggregate, compared with the wild-type protein, provide strong support for a direct and critical role of α-synuclein aggregation in the etiology of Parkinson's disease. Parenthetically, it might be noted that the involvement of α-synuclein in Parkinson's disease arose from gene-linkage experiments in familial early-onset Parkinson's disease, which revealed the A53T mutation.

REFERENCES

1. Lewy, F. H. (1912) *Handb. Neurol. 3*, 920−933.
2. Forno, L. S. (1996) *J. Neuropathol. Exp. Neurol. 55*, 259−272.
3. Okazaki, H., Lipkin, L. E., and Aronson, S. M. (1961) *J. Neuropathol. Exp. Neurol. 21*, 442−449.
4. Trojanowski, J. O., Goedert, M., Iwatsubo, T., and Lee, V. M.-Y. (1998) *Cell Death Diff. 5*, 832−837.
5. Duffy, P. E., and Tennson V. M. (1965) *J. Neuropathol. Exp. Neurol. 24*, 398−414.
6. Spillantini, M. G., Schmidt, M. L., Lee, V. M.-Y., Trojanowski, J. O., Jakes, R., and Goedert, M. (1997) *Nature (London) 388*, 839−840.
7. Spillantini, M. G., Growther, R. A., Jakes, R., Hasegawa, M., and Goedert, M. (1998) *Proc. Natl. Acad. Sci. U.S.A. 95*, 6469−6473.
8. Polymeropoulos, M. H., Lavedan, C., Leroy, E., Ide, S. E., Dehejia, A., Dutra, A., Pike, B., Root, H., Rubenstein, J., Boyer, R., Stenroos, E. S., Chandrasekharappa, S., Athanassiadou, A., Papapetropoulos, T., Johnson, W. G., Lazzarini, A. M., Duvoisin, R. C., Di Iorio, G., Golbe, L. I., and Nussbaum, R. L. (1997) *Science 276*, 2045−2047.
9. Krüger, R., Kuhn, W., Muller, T., Woitalla, D., Graeber, M., Kosel, S., Przuntek, H., Epplen, J. T., Schols, L., and Riess, O. (1998) *Nat. Genet. 18*, 106−108.
10. Masliah, E., Rockenstein, E., Veinbergs, I., Mallory, M., Hashimoto, M., Takeda, A., Sagara, Y., Sisk, and A. Mucke, L. (2000) *Science 287*, 1265−1269.
11. Feany, M. B., and Bender, W. W. (2000) *Nature 404*, 394−398.
12. Maroteaux, L., Campanelli, J. T., and Scheller, R. H. (1988) *J. Neurosci. 8*, 2804−2815.
13. Jakes, R., Spillantini, M. G., and Goedert, M. (1994) *FEBS Lett. 345*, 27−32.
14. Iwai, A., Masliah, E., Yoshimoto, M., Ge, N., Flanagan, L., de Silva, H. A., Kittel, A., and Saitoh, T. (1995) *Neuron 14*, 467−475.
15. George, J. M., Jin, H., Wood, W. S., and Clayton, D. F. (1995) *Neuron 15*, 361−372.
16. Hsu, L. J., Mallory, M., Xia, Y., Veinbergs, I., Hashimoto, M., Yoshimoto, M., Thal, L. J., Saitoh, T., and Masliah, E. (1998) *J. Neurochem. 71*, 338−344.
17. Goedert, M. (1997) *Nature (London) 388*, 232−233.
18. Weinreb, P. H., Zhen, W. G., Poon, A. W., Conway, K. A., and Lansbury, P. T., Jr. (1996) *Biochemistry 35*, 13709−13715.
19. Uversky, V. N., Li, J., and Fink, A. L. (2001) *J. Biol. Chem. 276*, 10737−10744.
20. Uversky, V. N., Gillespie, J. R., and Fink, A. L. (2000) *Proteins: Struct., Funct., Genet. 42*, 415−327.
21. Conway, K. A., Harper, J. D., and Lansbury, P. T. (1998) *Nat. Med. 4*, 1318−1320.
22. Crowther, R. A., Jakes, R., Spillantini, M. G., and Goedert, M. (1998) *FEBS Lett. 436*, 309−312.
23. El-Agnaf, O. M. A., Jakes, R., Curran, M. D., and Wallace, A. (1998) *FEBS Lett. 440*, 67−70.
24. Narhi, L., Wood, S. J., Steavenson, S., Jiang, Y., Wu, G. M., Anafi, D., Kaufman, S. A., Martin, F., Sitney, K., Denis, P., Louis, J. C., Wypych, J., Biere, A. L., and Citron, M. (1999) *J. Biol. Chem. 274*, 9843−9846.
25. Giasson, B. I., Uryu, K., Trojanowski, J. Q., and Lee, V. M. (1999) *J. Biol. Chem. 274*, 7619−7622.
26. Wood, S. J., Wypych, J., Steavenson, S., Louis, J. C., Citron, M., and Biere, A. L. (1999) *J. Biol. Chem. 274*, 19509−19512.
27. Conway, K. A., Harper, J. D., and Lansbury, P. T. (2000) *Biochemistry 39*, 2552−2563.
28. Conway, K. A., Lee, S. J., Rochet, J. C., Ding, T. T., Williamson, R. E., and Lansbury, P. T. (2000) *Proc. Natl. Acad. Sci. U.S.A. 97*, 571−576.
29. Serpell, L. C., Berriman, J., Jakes, R., Goedert, M., and Crowther, R. A. (2000) *Proc. Natl. Acad. Sci. U.S.A. 97*, 4897−4902.
30. Naiki, H., Higuchi, K., Hosokawa, M., and Takeda, T. (1989) *Anal. Biochem. 177*, 244−249.
31. Naiki, H., Higuchi, K., Matsushima, K., Shimada, A., Chen, W. H., Hosokawa, M., and Takeda, T. (1990) *Lab. Invest. 62*, 768−773.
32. Oberg, K., Chrunyk, B. A., Wetzel, R., and Fink, A. L. (1994) *Biochemistry 33*, 2628−2634.
33. Oberg, K. A., and Fink, A. L. (1998) *Anal. Biochem. 256*, 92−106.
34. Wakatsuki, S., Hodgson, K. O., Eliezer, D., Rice, M., Hubbard, S., Gillis, N., and Doniach, S. (1992) *Rev. Sci. Instrum. 63*, 1736−1740.
35. Tsuruta, H., Brennan, S., Rek, Z. U., Irving, T. C., Tompkins, W. H., and Hodgson, K. O. (1998) *J. Appl. Crystallogr. 31*, 672−682.
36. Glatter, O., and Kratky, O. (1982) *Small-angle X-ray scattering*, Academic Press, New York.
37. Tanford, C., De, P. K., and Taggart, V. G. (1960) *J. Am. Chem. Soc. 82*, 6028−6034.
38. Tanford, C. (1968) *Adv. Protein Chem. 23*, 121−282.
39. Arakawa, T., and Goddette, D. (1985) *Arch. Biochem. Biophys. 241*, 21−32.
40. Wilkinson, K. D., and Mayer, A. N. (1986) *Arch. Biochem. Biophys. 250*, 390−399.
41. Jackson, M., and Mantsch, H. H. (1992) *Biochim. Biophys. Acta 1118*, 139−143.

42. Dufour, E., Bertrand-Harb, C., and Haertle, T. (1993) *Biopolymers 32*, 589−598.
43. Buck, M., Radford, S. E., and Dobson, C. M. (1993) *Biochemistry 32*, 669−678.
44. Fan, P., Bracken, C., and Baum, J. (1993) *Biochemistry 32*, 463−479.
45. Thomas, P. D., and Dill, K. A. (1993) *Protein Sci. 2*, 2050−2065.
46. Alexandrescu, A. T., Ng, Y.-L., and Dobson, C. M. (1994) *J. Mol. Biol. 235*, 587−599.
47. Hamada, D., Kuroda, Y., Tanaka, T., and Goto, Y. (1995) *J. Mol. Biol. 254*, 737−746.
48. Bychkova, V. E., Dujsekina, A. E., Klenin, S. I., Tiktopulo, E. I., Uversky, V. N., and Ptitsyn, O. B. (1996) *Biochemistry 35*, 6058−6063.
49. Kamatari, Y. O., Konno, T., Kataoka, M., and Akasaka, K. (1996) *J. Mol. Biol. 259*, 512−523.
50. Uversky, V. N., Narizhneva, N. V., Kirschstein, S. O., Winter, S., and Lober, G. (1997) *Folding Des. 2*, 163−172.
51. Narizhneva, N. V., and Uversky, V. N. (1997) *Protein Pept. Lett. 4*, 243−249.
52. Dahlman Wright, K., Baumann, H., McEwan, I. J., Almlöf, T., Wright, A. P., Gustafsson, J. A., and Härd, T. (1995) *Proc. Natl. Acad. Sci. U.S.A. 92*, 1699−1703.
53. Schmitz, M. L., dos Santos Silva, M. A., Altmann, H., Czisch, M., Holak, T. A., and Baeuerle, P. A. (1994) *J. Biol. Chem. 269*, 25613−25620.
54. Donaldson, L., and Capone, J. P. (1992) *J. Biol. Chem. 267*, 1411−1414.
55. Baskakov, I., and Bolen, D. W. (1998*) J. Biol. Chem. 273*, 4831−4834.
56. Baskakov, I. V., Kumar, R., Srinivasan, G., Ji, Y. S., Bolen, D. W., and Thompson, E. B. (1999) *J. Biol. Chem. 274*, 10693−10696.
57. Davidson, W. S., Jonas, A., Clayton, D. F., and George, J. M. (1998) *J. Biol. Chem. 273*, 9443−9449.
58. Uversky, V. N., Segel, D. J., Doniach, S., and Fink, A. L. (1998) *Proc. Natl. Acad. Sci. U.S.A. 95*, 5480−5483.
59. Uversky, V. N., Khurana, R., Karnoup, A. S., Segel, D., Doniach, S., and Fink, A. L. (1999) *Protein Sci. 8*, 161−173.
60. Ismail, A. A., Mantsch, H. H., and Wong, P. T. T. (1992) *Biochim. Biophys. Acta 1121*, 183−188.
61. Przybycien, T. M., Dunn, J. P., Valax, P., and Georgiou, G. (1994) *Protein Eng. 7*, 131−136.
62. Kendrick, B. S. Cleland, J. L., Lam, X., Nguyen, T., Randolph, T. W., Manning, M. C., and Carpenter, J. F. (1998) *J. Pharm. Sci. 87*, 1069−1076.
63. Clark, A. H., Saunderson, D. H., and Suggett, A. (1981) *Int. J. Pept. Protein Res. 17*, 353−364.
64. Fink, A. L. (1998) *Folding Des. 3*, 9−15.
65. Nielsen, L., Frokjaer, S., Carpenter, J. F., and Brange J. (2001) *J. Pharm. Sci. 90*, 29−37.
66. Khurana, R., Oberg, K. A., Seshadri, S., Li, J., and Fink, A. L. (2001) *Proc. Natl. Acad. Sci. U.S.A.* (submitted for publication).
67. Kyte, J., and Doolittle, R. F. (1982) *J. Mol. Biol. 157*, 105−132.
68. Guermeur, Y. (1997) Combinaison de classifeurs statistiques, Application a la prediction de structure secondaire des proteines, Ph.D. Thesis, University of Paris.

BI010616G